Effect of stirring rate on the morphology of FDU-12 mesoporous silica particles

CrossMark

Silo Meoto [a], Niall Kent [a], Michael M. Nigra [b], Marc-Olivier Coppens [a, *]

[a] *Department of Chemical Engineering, University College London, Torrington Place, London, WC1E 7JE, United Kingdom*
[b] *Department of Chemical Engineering, University of Utah, Salt Lake City, UT 84112, United States*

ARTICLE INFO

ABSTRACT

Ordered mesoporous FDU-12 silica particles with different morphologies were synthesized by varying the stirring rate. The mesoporous structure and textural properties of the FDU-12 samples were characterized by N_2 adsorption and desorption, scanning electron microscopy, transmission electron microscopy and small angle X-ray scattering. The influence of the stirring conditions on the morphology was demonstrated, as the FDU-12 particle morphology changes from a regular, hexagonal platelet to a poorly defined shape when the stirring rate is changed from slow to fast. At very fast stirring rate, shear influences the mesophase structure, although the pore diameter and wall thickness remain unchanged.

1. Introduction

Ordered mesoporous silica materials are applied in catalysis [1,2], molecular adsorption [3,4] and separation [5]. In addition to their internal textural properties (ordered and adjustable pore size, large surface area and pore volume), the external morphology of these materials also affects their applicability. Over the years, many different ordered mesoporous silica materials have been reported, including MCM-41, MCM-48, SBA-15, SBA-16 and FDU-12 [6–10], with different morphological and topological characteristics, which allow for an extensive range of potential applications. For instance, mesoporous silica fibres and nanotubes with aligned one-dimensional (1D) pores, such as MCM-41, can be used in nanofluidic applications or to template nanorods. However, mesoporous materials with a three-dimensional (3D) pore network system, such as MCM-48, SBA-16, KIT-5, FDU-1 and FDU-12, are advantageous for processes limited by diffusion or prone to pore blockage, for example in catalysis or separation processes, compared to materials with 1D channels [11]. 3D mesoporous materials, with pore networks templated by micellar cubic phases, contain large cavities or cages connected by multidirectional pore entrances of smaller sizes (so-called windows). The pore system is templated by micelles formed by a block copolymer. The cavity and window size can be controlled by adjusting the synthesis and hydrothermal treatment conditions, such as the temperature, or by adding the right amount of swelling agent [12].

Different acidic synthesis procedures lead to the formation of fibres, spheres, and mesoporous silica films [8,13–15]. The optimal morphology depends on the application. For example, films are useful for gas sensing [16], while mesoporous spheres are desirable for catalytic and adsorption processes, as this shape facilitates their packing in fixed bed reactors or in liquid chromatography, as the stationary phase [17]. Tailoring particle morphology is therefore critical to the envisioned application of a mesoporous silica material.

Mesoporous silica with a uniform cubic array of spherical mesopores was first reported in 1998 by Zhao et al. [6,14,15] A cubic ($Im\overline{3}m$) cage-like mesostructured silica, SBA-16, with pore size of ca. 5 nm, was synthesized using triblock copolymer Pluronic F127 [$EO_{106}PO_{70}EO_{106}$ — where EO = poly(ethylene oxide) and PO = poly(propylene oxide)] and star diblock copolymers [6]. The same triblock copolymer was used to make mesoporous silica fibres with a 3D cage structure, in a hexagonal arrangement, and a pore size ranging from 4 to 6 nm [14]. Subsequent studies focused on expanding the size of these mesopores. Fan et al. synthesized large-pore (up to 13 nm) mesoporous silica with face-centred cubic ($Fm\overline{3}m$) structure, denoted as FDU-12 [11]. Mesoporous FDU-12 is synthesized in an acidic solution using the same non-ionic triblock

* Corresponding author.
E-mail address: m.coppens@ucl.ac.uk (M.-O. Coppens).

copolymer Pluronic F127 as the template, together with 1,3,5-trimethylbenzene (TMB) and potassium chloride (KCl) as additives, and tetraethylorthosilicate (TEOS) as the silica source. The organic TMB acts as a swelling agent to increase the cavity and window sizes. It was suggested that TMB enters the hydrophobic part of the micelles and increases the volumetric ratio of the hydrophobic core to the hydrophilic corona, which leads to a phase transformation from a body-centred cubic structure ($Im\bar{3}m$) to a face-centred cubic structure ($Fm\bar{3}m$) [11]. A novel low-temperature synthetic pathway was then developed to synthesize ordered mesoporous FDU-12 with very large pore sizes, up to 27 nm [18]. Fan et al. decreased their synthesis temperature to as low as 15 °C, which allowed them to make highly ordered cubic ($Fm\bar{3}m$) silica structures with a pore diameter in the range of 22–27 nm. Kruk and Hui [19] improved on this low-temperature procedure for FDU-12 silica, so that materials with good structural ordering and narrow pore size distribution could be obtained from a wider range of low temperatures than originally proposed by Fan et al. The selection of their synthesis conditions made it possible to tailor both the cavity and window sizes. The size of the pore entrance is also important to applications in which diffusion rates matter, and can be adjusted in the range of 4–9 nm by tailoring the hydrothermal treatment temperature [11,12,19].

Several investigations on the effect of the synthesis conditions of FDU-12, such as synthesis temperature, hydrothermal temperature and duration, silica concentration, acid concentration, and salt concentration have been carried out. The concentration of HCl and the type of salt used can influence the formation of the silica particles [20–22]. As discussed, much effort has been devoted to controlling the characteristics of the mesostructure, such as the pore cavity and window sizes of mesoporous silica with cage-like structures, but very little has been reported on controlling the external morphology or macrostructure of FDU-12 silica particles. Better understanding of methods to tune the morphology would allow more precise control over properties that are relevant to specific applications. Several studies have linked the interaction between hydrolysed silicic species and the micelles formed during the gel phase and hydrothermal treatment, to the growth of a mesoporous silica particle [23,24]. Chan et al. first proposed a realistic phase separation model for the mechanism of formation of silica mesostructured precipitates [25], which was further developed by Yu et al. for a non-ionic block copolymer templating system [26]; it suggests that mesoporous materials are formed in three stages: cooperative self-assembly of inorganic/organic composites, formation of a liquid crystal-like phase of block copolymer/silica aggregates, and phase separation of the liquid crystal-like phase from the solution with condensation of silica species driving the growth of the solid mesostructures. According to this mechanism, the particle shape ultimately results from competition between the free energy of mesostructural self-assembly, the colloidal surface free energy, and energy imparted by other interactions, such as shear.

A few reports have explored the effect of not stirring (static conditions) [9,26] or stirring for different times [22,27]. Huang et al. studied the effect of different swelling agents (xylene, toluene, and TMB), time and temperature of synthesis, different silica sources (TEOS versus TMOS), effect of salt (KCl) and the silica/surfactant ratio, but kept the stirring rate constant at 350 rpm or varied within a narrow range between 370 and 450 rpm [28,29]. Therefore, no reports have mentioned the effect of the stirring rate during synthesis on the formation and morphology of FDU-12 mesoporous silica. As will be shown, the stirring rate is not a trivial factor. It is one that can govern the structure of these silica materials and influence the uniformity of the macroscopic shape. The aim of this study is to demonstrate the effect of the stirring rate on the resultant particle morphology and porous parameters of F127-templated porous silica material.

2. Experimental section

2.1. Chemicals

Tetraethylorthosilicate (TEOS, reagent grade 98% purity), Pluronic F127 [poly(ethylene oxide)-poly(propylene oxide)-poly(ethylene oxide) tri-block copolymer $EO_{106}PO_{70}EO_{106}$], hydrochloric acid (HCl, analytical grade 37 wt%), trimethylbenzene (TMB, analytical reagent 98% purity), and potassium chloride (KCl, 99 wt %) were purchased from Sigma Aldrich Company Ltd. (Dorset, UK).

2.2. Synthesis

The synthesis procedure was performed based on the report in Ref. [11]. First, 2.0 g of Pluronic F127 was dissolved in a mixture with 2.0 g of TMB, 5.0 g of KCl and 120 ml of 2 M HCl and stirred for 24 h at 40 °C. Then, 8.3 g of TEOS was added to the reaction mixture, and stirred at different rates or left under static conditions for 24 h at 40 °C. The different stirring conditions are listed in Table 1. Stirring was conducted using an oval magnetic stir bar. The mixture was then transferred to a convection oven for hydrothermal treatment at 100 °C for 72 h. Thereafter, the solid product was filtered, washed three times with deionized water, and dried at room temperature overnight. The material was calcined at 550 °C for 6 h to obtain the mesoporous silica. The resulting mesoporous silica samples were designated FDU-12-X, where X indicates the stirring rate, e.g., FDU-12-100 for X = 100 rpm.

2.3. Characterization methods

Scanning electron microscopy was performed with a JEOL JSM-6480LV high-performance SEM (JEOL, Tokyo, Japan). The samples for SEM were sputter-coated with gold for 90 s before imaging, to reduce charging. Transmission electron microscopy (TEM) was performed with a JEOL 2100 200 kV TEM (Tokyo, Japan) with a Gatan camera (Pennsylvania, USA). The samples for TEM were prepared as a suspension in methanol and dropped on a 300-mesh copper grid with a carbon film. Powder X-ray diffraction (XRD) patterns were measured with a Stoe Stadi-P copper anode capillary transmission powder X-ray diffractometer in the range of 0.5–3°. Nitrogen adsorption and desorption isotherms were obtained with an Autosorb-iQ-MP-XR (Quantachrome, Florida, USA) at −196.15 °C with samples outgassed at 300 °C for 8 h with a pre-treatment at 100 °C for 2 h. Argon adsorption and desorption isotherms for micropore analysis were obtained at −186.15 °C using the same Quantachrome instrument. The pore size distribution was

Table 1
Sample nomenclature, corresponding to different stirring conditions.

Sample	Stirring rate (rpm)
FDU-12-80′	Shaking, ~80 (no pellet)
FDU-12-0	Static, 0 (after 10 min of stirring)
FDU-12-100	100
FDU-12-200	200
FDU-12-300	300
FDU-12-400	400
FDU-12-500	500
FDU-12-600	600
FDU-12-700	700
FDU-12-800	800
FDU-12-900	900
FDU-12-1000	1000

calculated from the adsorption branch of an isotherm by the nonlocal density functional theory (NLDFT) analysis method using a spherical model for the pore cavities and the BET surface area was calculated based on relative pressures $P/P_0 = 0.05–0.3$. The micropore analysis was obtained from the argon adsorption data.

3. Results and discussion

SEM images of the samples synthesized using different stirring rates are shown in Fig. 1. Mainly agglomerates are observed in these images. Particles synthesized in the absence of stirring (FDU-12-0 in Fig. 1(a)), under mild shaking (FDU-12-80′ in Fig. S1(a)) or under mild stirring (FDU-12-100 in Fig. 1(b), FDU-12-200 in Fig. S1(b)) have the best defined polyhedral shapes. These silica particles consistently have a hexagonally edged platelet structure, which is 1.6–2.6 μm in size. In contrast, when the stirring rate is increased beyond 200 rpm, more and more irregularly shaped particles are formed. Samples FDU-12-500 and FDU-12-800 are aggregates composed of poorly defined particles with some composed of the smaller platelets (Fig. 1(c)) or large spheroidal particles (see Fig. S1(e), Supplementary Information). It is difficult to attribute a particle size to these samples, because of the agglomeration of the primary particles. Monodisperse spheres were not obtained at any stirring rate. Literature reports show that SBA-16, which is also templated with F127, can form particles of a uniform spherical shape [27,30–32]. This spherical shape was transformed to a polyhedral shape by increasing reaction time beyond 60 min (decaoctahedral) and 120 min (rhombdodecahedral) after stirring for 30 min [27] or by varying the surfactant/silica (F127/TEOS) molar ratio, acid concentration and temperature [30]. Fan et al. [11] also reported FDU-12 silica with a spherical morphology. However, this spherical morphology was achieved for particles synthesized at a higher temperature (100 °C). Yuan et al. [33] succeeded in forming an FDU-12 material with facets similar to those seen in FDU-12-0 and FDU-12-100 with a surfactant/silica

molar ratio of 0.004. Although their choice of surfactant was different (F108), the result achieved was similar to that obtained with the F127/TEOS molar ratio of 0.004 for this synthesis.

Previous work have shown that the morphology of mesoporous silica particles is derived from the shape of the block copolymer micelles, which is influenced by the synthesis recipe and preparation procedure. Sayari et al. [9] showed that, to produce short, monodisperse SBA-15 rods, it is essential not to stir the synthesis mixture. Zu et al. [34] showed that platelet-like SBA-15 particles are generated when the time of the micelle formation process is short and the stirring rate is high (>800 rpm), while a rod-like morphology is obtained when the micelle formation time is long (several hours), regardless of stirring rate. Hwang et al. [27] determined an optimal stirring time of 30 min in order to yield well-defined, microwave-synthesized, cubic SBA-16 particles. In our synthesis procedure, samples are stirred for 24 h. A long stirring time at high stirring rates may cause the silica particles to overgrow, leading to the undefined shapes observed at higher stirring rates (>200 rpm). Mesa et al. [30] explained that, for F127/TEOS systems, a gel-like phase is obtained for the silica particles at temperatures of 40 °C or lower, regardless of the F127/TEOS molar ratio. The well-defined shapes seen under static or low stirring rate conditions bears similarities to what is observed when synthesizing rod-shaped SBA-15 particles, which are obtained only under static conditions [9].

Interestingly, however, the external morphologies do not reflect the internal structure of the samples. The porous structure was studied by measuring nitrogen adsorption and desorption isotherms. The results are shown in Fig. 2, Figs. S2 and S3. The textural properties of all samples are listed in Table 2 and Table S1.

All samples show a type IV isotherm, characteristic of an ordered mesoporous material. The delay in desorption and steepness of the desorption isotherm around the relative pressure $P/P_0 = 0.45$ suggests that the material has a cage-like pore structure. The hysteresis loops of all samples occur over the relative pressure range of
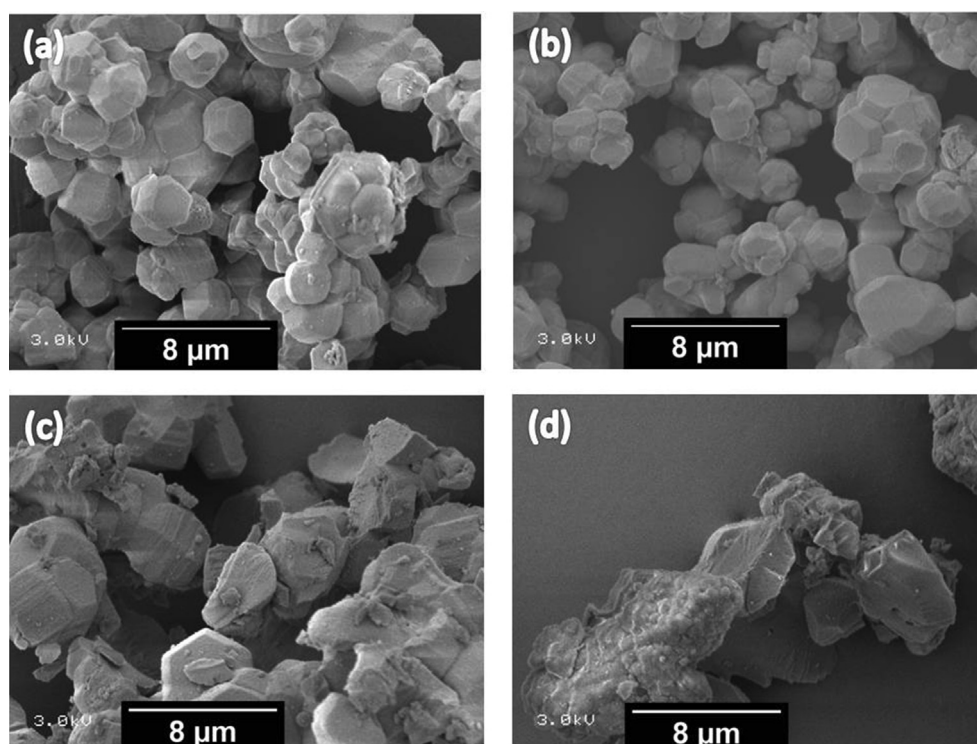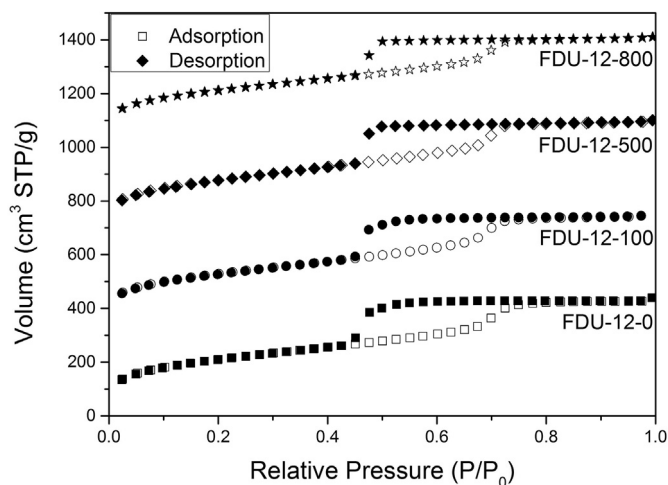

Fig. 1. SEM images of FDU-12 samples synthesized at different stirring rates and conditions: (a) FDU-12-0, (b) FDU-12-100, (c) FDU-12-500 and (d) FDU-12-800.

Fig. 2. Nitrogen adsorption/desorption isotherms of FDU-12 samples. The isotherms for FDU-12-100, -500, and -800 samples are shifted upwards by 331, 670, and 1022 cm³ STP/g respectively.

0.4–0.75 and are of H_2 type, where the steep desorption branch and smooth adsorption branch of this hysteresis loop can be associated to pore-blocking due to pore entrances or windows that are much narrower than the cages to which they lead. The results show that the stirring rate has a negligible effect on the textural parameters. The majority of the samples have a pore (cavity or cage) diameter of approximately 10.2 ± 0.3 nm. The pore size distribution is given in Fig. 3. Within statistical errors, Fig. 3 shows a nearly identical, narrow bimodal pore size distribution for all samples with two

peaks corresponding to, respectively, the cavities and windows. The window size is determined by NLDFT to be ~2.5 nm. The BET surface area of the materials ranges from 542 to 716 m²/g, and the total pore volume from 0.52 to 0.68 cm³/g. The micropore volume was determined with argon adsorption to be ~0.25 cm³/g. This demonstrates that the pore structure is uniform and reproducible.

SAXS patterns of selected calcined samples are shown in Fig. 4. The SAXS patterns were collected in the q range from 0.009 to 0.7 Å⁻¹. The patterns of the samples show well-resolved peaks, which are assigned to be (111), (311), (222), (331), (420), (440) and (531) Miller indices. These peaks correspond to diffraction from a face-centred cubic (*fcc*) structure, with a space group of $Fm\overline{3}m$. Along with the N_2 adsorption/desorption measurement results, this confirms the material as FDU-12.

The unit cell size, a_0, was calculated from the (111) peak position for these samples (Table 3), using the expression:

$$q = \frac{2\pi}{a_0} \sqrt{h^2 + k^2 + l^2} \qquad (1)$$

with (hkl) = (111).

The results show that there is only a very slight change in the unit cell dimension, indicating that the unit cell remains unchanged, whether stirring or not, and at any stirring rate.

The lower-indexed, intense Bragg peaks are somewhat broadened due to polydispersity and disorder. Crystal defects in a crystalline material could also contribute to peak broadening. Assuming that the broadening arises solely from the ordered structure, a domain size is estimated from Scherrer's equation using the full width at half-maximum (FWHM) power of the most intense peak (111) to be 39, 35, 36, and 38 nm for FDU-12-0, -100,

Table 2
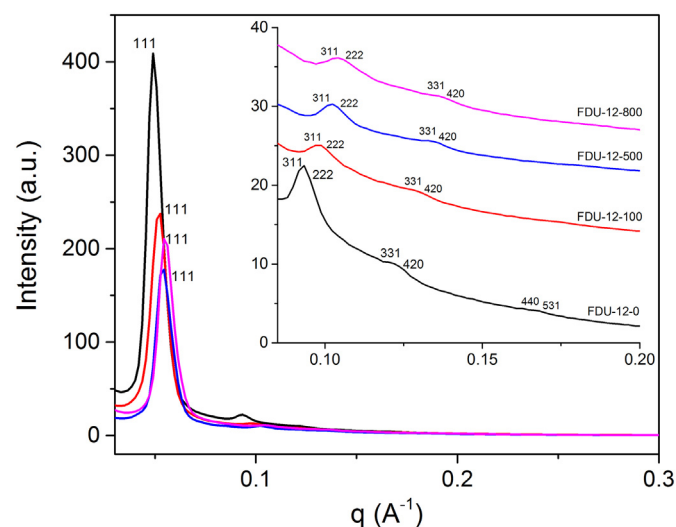Textural properties of the samples determined from N_2 adsorption/desorption measurements.

Sample	BET surface area (m²/g)	Pore volume (cm³/g)	Cavity diameter (nm)[a]	Window size (nm)[b]
FDU-12-0	716	0.68	10.1	2.45
FDU-12-100	680	0.64	10.1	2.49
FDU-12-500	716	0.67	10.1	2.45
FDU-12-800	654	0.60	10.1	2.45

[a] Calculated from the N_2 adsorption isotherm, based on the NLDFT model, assuming a spherical shape for the pore cavities (corresponds to the second maximum in Fig. 3).
[b] Determined from the pore size distribution calculated from the adsorption branch of the isotherms based on NLDFT mode (correspond to the first maximum in Fig. 3).
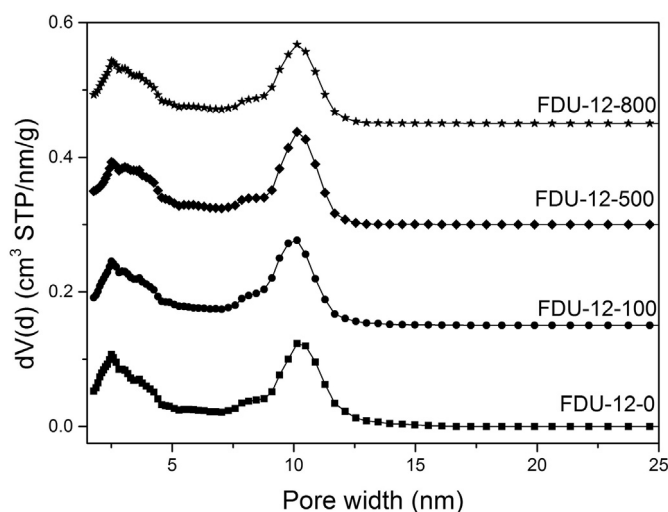
Fig. 3. NLDFT pore size distribution of FDU-12 samples, showing the cavity diameter and window size. Curves for FDU-12-100, -500, and -800 samples are shifted upwards by 0.15, 0.3, and 0.45 cm³ STP/nm/g, respectively.

Fig. 4. SAXS patterns of FDU-12 samples. Inset: region between 0.085 and 0.2 Å⁻¹, where the curves for FDU-12-100, -500, -800 samples are shifted upwards by 12, 20 and 25 a.u., respectively.

Table 3
Textural properties determined from SAXS.

Sample	d_{111} (nm)	a_0 (nm)	Pore wall thickness (nm)
FDU-12-0	11.9	20.7	4.5
FDU-12-100	11.6	20.1	4.1
FDU-12-500	11.6	20.1	4.1
FDU-12-800	11.6	20.1	4.1

d_{111} was calculated from the peak maximum. a_0 was calculated from Eqn. (1). Minimum pore wall thickness (see Supplementary Information).

-500, -800 samples respectively. Here, the domain size represents the lower limit for which stirring affects the macroscopic morphology.

TEM micrographs were obtained to observe the internal structure and mesophase of all the samples. The images generally reveal large domains of well-aligned, ordered pores, which is in agreement with the SAXS results. The cubic phase of these structures is clearly seen (Fig. 5), corresponding to the *fcc* structure resolved using SAXS. The FDU-12-800 sample (Fig. 5(D)) shows regions with a more disordered arrangement of pores. This is seen in FDU-12-1000 as well (Fig. S6 in the Supplementary Information), indicating that a very high stirring rate (>800 rpm) is detrimental to the formation of a long-distance periodically ordered mesostructure, even though neither the pore diameter nor the local organisation, as illustrated by SAXS, are affected.

Stirring induces shear, which plays a role in the formation of the particles, and affects, in particular, their shape. The results show that the pore diameter of the samples remains essentially unchanged, and the unit cell size a_0 for all samples is similar. However, there are differences in the particle morphology and also in the mesophase organisation, especially at very high stirring rate. This means that fast stirring may influence the surfactant/silica species interactions, albeit only slightly. The platelet shape is different from cubic mesoporous silica materials, where the spherical micelles nucleate, grow and aggregate into spheroidal or cubic structures. The materials formed under slow stirring conditions have a unique morphology. The following hypothesis is proposed to explain the disparity observed in the particle morphology. When shaking, stirring slowly, or under static conditions, micelles can nucleate and grow in a more stable environment. When stirring rapidly, however, shear on the micelles is pronounced, so that micellar growth is hindered, as well as the assembly with silica precursors to grow large, well defined particles with long-range order of the mesopores. Poorly defined morphologies result from rapid reorganisation or reassembly of growing particles.

With no change in mesostructure observed, it would seem that this material, FDU-12, is more robust under shear than other previously studied materials, such as SBA-15. Literature shows that the P123 block copolymer gives a variety of mesostructures, depending on concentration and other synthesis parameters. In particular, the cylindrical, elongated P123 micelles of the SBA-15 system are more sensitive to shear during SBA-15 synthesis. The F127 block copolymer, on the other hand, primarily yields less extended, spherical micelles. This could be the cause for the robustness of the ultimately formed material structures seen in this study and highlights an essential difference with SBA-15 synthesis.
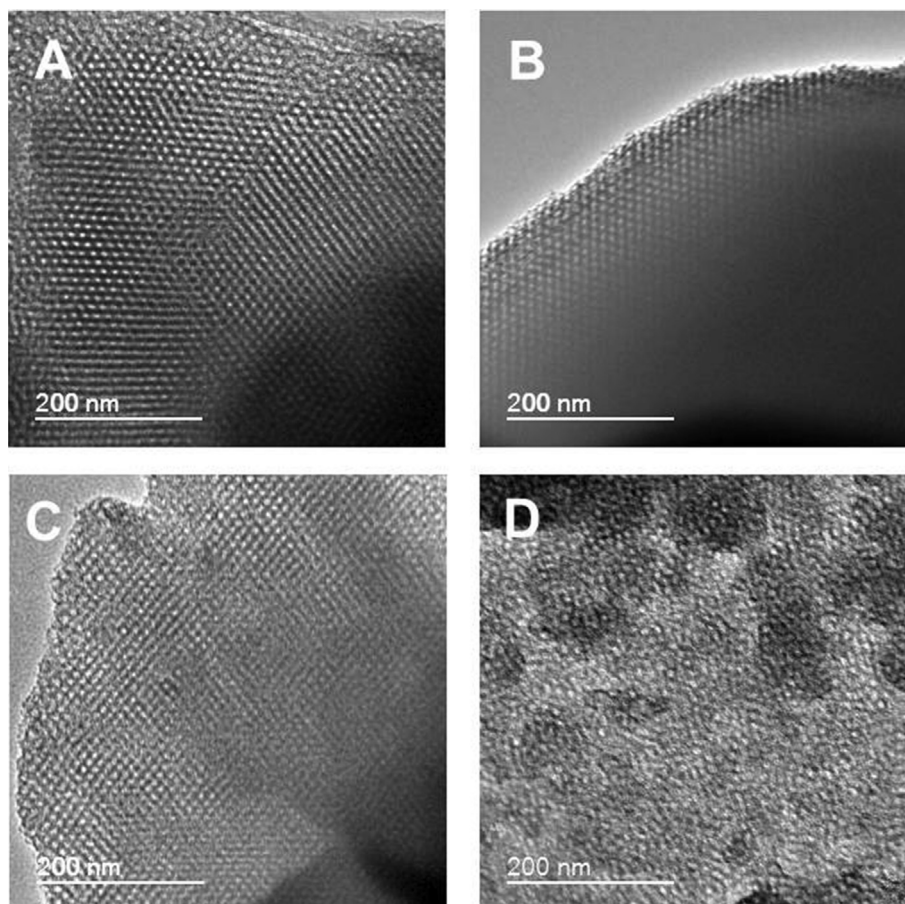
Fig. 5. TEM images of samples (A) FDU-12-0, (B) FDU-12-100, (C) FDU-12-500 and (D) FDU-12-800.

4. Conclusion

It was shown that the stirring rate can be employed to tailor the particle morphology of mesoporous silica particles with 3D cubic mesoscopic order. Different stirring rates lead to different shear rates that, in turn, influence the aggregation of primary particles, as well as the growth of the silica mesophase. Shear, influenced by the stirring rate, can affect the growth of the silica particles and, consequently, the evolution of the structures formed, inside a confined space. Well-defined shapes are observed at lower stirring rates, including static conditions, while higher stirring rates lead to indistinct shapes. It appears that, for the synthesis of ordered mesoporous silica in the granular state, reaction conditions such as temperature and composition determine the internal structure while the stirring rate has much less effect on the textural parameters, but will affect the final particle morphology. This matters, since three-dimensionally connected pore networks, such as those in FDU-12, are beneficial to applications in separations and catalysis, because they ensure accessibility of the internal volume and are less affected by pore blockage.

Acknowledgements

Appendix A. Supplementary data

Supplementary data related to this article can be found at http://dx.doi.org/10.1016/j.micromeso.2017.04.045.

References

[1] Q. Yang, J. Liu, J. Yang, M.P. Kapoor, S. Inagaki, C. Li, J. Catal. 228 (2004) 265–272.
[2] B. Rac, M. Nagy, I. Palinko, A. Molnar, Appl. Catal. A Gen. 316 (2007) 152–159.
[3] W.-C. Chang, J.R. Deka, H.-Y. Wu, F.-K. Shieh, S.-Y. Huang, H.-M. Kao, Appl. Catal. B Environ. 142–143 (2013) 817–827.
[4] Y. Zhou, J. Yang, J.Y. Yang, F.N. Gu, Y. Wang, J.H. Zhu, J. Mater. Chem. 21 (2011) 13895.
[5] S. Wu, J. Wang, G. Liu, Y. Yang, J. Lu, J. Memb. Sci. 390–391 (2012) 175–181.
[6] D. Zhao, Q. Huo, J. Feng, B.F. Chmelka, G.D. Stucky, J. Am. Chem. Soc. 120 (1998) 6024–6036.
[7] T. Kim, F. Kleitz, B. Paul, R. Ryoo, J. Am. Chem. Soc. 127 (2005) 7601–7610.
[8] D. Zhao, J. Sun, Q. Li, G.D. Stucky, S. Barbara, Chem. Mater. 12 (2000) 275–279.
[9] A. Sayari, B. Han, Y. Yang, JACS 126 (2004) 14348–14349.
[10] O.C. Gobin, Y. Wan, D. Zhao, F. Kleitz, S. Kaliaguine, J. Phys. Chem. C 111 (2007) 3053–3058.
[11] J. Fan, C. Yu, F. Gao, J. Lei, B. Tian, L. Wang, Q. Luo, B. Tu, W. Zhou, D. Zhao, Angew. Chem. Int. Ed. 42 (2003) 3146–3150.
[12] T. Yu, H. Zhang, X. Yan, Z. Chen, X. Zou, P. Oleynikov, D. Zhao, J. Phys. Chem. B 110 (2006) 21467–21472.
[13] S.K. Seshadri, H.M. Alsyouri, Y.S. Lin, J. Mater. Sci. 48 (2013) 7042–7054.
[14] P. Yang, D. Zhao, B.F. Chmelka, G.D. Stucky, Chem. Mater. 10 (1998) 2033–2036.
[15] D. Zhao, P. Yang, N. Melosh, J. Feng, B.F. Chmelka, G.D. Stucky, Adv. Mater. 10 (1998) 1380–1385.
[16] T. Yamada, H.S. Zhou, H. Uchida, M. Tomita, Y. Ueno, T. Ichino, I. Honma, K. Asai, T. Katsube, Adv. Mater. 14 (2002) 812–815.
[17] C. Boissière, M. Kümmel, M. Persin, A. Larbot, E. Prouzet, Adv. Funct. Mater. 11 (2001) 129–135.
[18] J. Fan, C. Yu, J. Lei, B. Tu, Q. Zhang, T. Li, W. Zhou, B. Tu, W. Zhou, D. Zhao, J. Am. Chem. Soc. 127 (2005) 10794–10795.
[19] M. Kruk, C.M. Hui, Microporous Mesoporous Mater. 114 (2008) 64–73.
[20] C. Yu, B. Tian, J. Fan, J. Am. Chem. Soc. 124 (2002) 4556–4557.
[21] F. Kleitz, D.N. Liu, G.M. Anilkumar, I.S. Park, L.A. Solovyov, A.N. Shmakov, R. Ryoo, J. Phys. Chem. B 107 (2003) 14296–14300.
[22] L.C. Cides da Silva, T.V.S. dos Reis, I.C. Cosentino, M.C.a. Fantini, J.R. Matos, R.E. Bruns, Microporous Mesoporous Mater. 133 (2010) 1–9.
[23] J.L. Blin, A. Léonard, B.L. Su, Chem. Mater. 13 (2001) 3542–3553.
[24] A. Léonard, J.L. Blin, M. Robert, P.A. Jacobs, A.K. Cheetham, B.L. Su, Langmuir 19 (2003) 5484–5490.
[25] H.B.S. Chan, P.M. Budd, T.D. Naylor, J. Mater. Chem. 11 (2001) 951–957.
[26] C. Yu, J. Fan, B. Tian, D. Zhao, Chem. Mater. 16 (2004) 889–898.
[27] Y.K. Hwang, J.S. Chang, Y.U. Kwon, S.E. Park, Microporous Mesoporous Mater. 68 (2004) 21–27.
[28] L. Huang, X. Yan, M. Kruk, Langmuir 26 (2010) 14871–14878.
[29] L. Huang, M. Kruk, Chem. Mater. 27 (2015) 679–689.
[30] M. Mesa, L. Sierra, J. Patarin, J.L. Guth, Solid State Sci. 7 (2005) 990–997.
[31] M. Mesa, L. Sierra, J.-L. Guth, Microporous Mesoporous Mater. 112 (2008) 338–350.
[32] M.A. Ballem, J.M. Córdoba, M. Odén, Microporous Mesoporous Mater. 129 (2010) 106–111.
[33] P. Yuan, J. Yang, X. Bao, D. Zhao, J. Zou, C. Yu, Langmuir 28 (2012) 16382–16392.
[34] S.-Z. Zu, L.-J. Mao, A. Sayari, B.-H. Han, J. Porous Mater. 19 (2012) 745–749.